Investigating the Influence of Operating Conditions on the Combined Steam and Carbon Dioxide Reforming of Methane Performance in the Presence of Ni/ZrO_2 Catalyst

Mosayebi, Amir*[+]

Department of Chemical Engineering, Tafresh University, Tafresh, I.R. IRAN

ABSTRACT: *In the present study, Ni/ZrO_2 catalyst was synthesized via a co-precipitation approach, and its catalytic activity was evaluated in Combined Steam and Carbon dioxide Reforming of Methane (CSCRM) reaction at a temperature range of 773 K–1273 K, CO_2:H_2O ratio of 0.5-3 and (CO_2 + H_2O)/CH_4 ratio of 0.5-3. The results demonstrated that the higher (CO_2+H_2O)/CH_4 ratio and temperature were required for CH_4 conversion of about 100%. The effect of CO_2/H_2O ratio was little on the CO and H_2 yield. A (CO_2+H_2O)/CH_4 ratio of 1.5 associated with CO_2/H_2O ratio of 0.5 at the minimum temperature of 1073 K was the required reaction condition for the synthesis gas (syngas) formation with H_2/CO ratio of about 2. The temperature, type, and amount of the oxidizing agent greatly affected the amount of coke deposition. The least temperature of 1073 K and (CO_2+H_2O)/CH_4 ratio higher than 1.5 irrespective of CO_2:H_2O ratio was obtained as proper operation conditions to avoid coke formation. Moreover, CO_2 revealed a higher portion than H_2O in coke formation in CSCRM reaction.*

KEYWORDS: *Ni/ZrO_2; Combined steam and carbon dioxide reforming of methane; Coke deposition; Gas to liquid; H_2/CO ratio.*

INTRODUCTION

In the refining process, Gas to Liquid (GTL) is used to convert natural gas or other gaseous hydrocarbons into longer-chain hydrocarbons, such as gasoline or diesel fuel [1]. Syngas formation, Fischer–Tropsch Synthesis (FTS), and product upgrading are the primary purposes of GTL [1]. Syngas production from natural gas has gained considerable interest in the chemical industries due to the existence of numerous problems such as depletion of hydrocarbon reserves, rising petroleum prices, and environmental aspects [2-3]. The central core of GTL the process is FTS, which is responsible for converting the syngas are derived from natural gas to clean environmental fuels with lower content of sulfur and aromatics [2]. Therefore designing the syngas production operation is absolutely critical to achieving a more economical profit for GTL process [3-4]. Methane, as a primary component of natural gas, is an energy source with low cost, and it is anticipated to extensively provide the energy demand in the forthcoming [4-6]. Syngas production *via* methane can be carried out using the three methods with

***** *To whom correspondence should be addressed.*
+ *E-mail*: *mosayebi@tafreshu.ac.ir*
1021-9986/2022/3/1061-1075 15/$/6.05

various compositions of H_2/CO including reaction with steam (SRM) [7-8], carbon dioxide (DRM) [9-10] and oxygen (POM) [11-13], which are described below:

$$CH_4 + H_2O \leftrightarrow CO + 3H_2 \quad (SRM) \quad (1)$$

$$CH_4 + CO_2 \leftrightarrow 2CO + 2H_2 \quad (DRM) \quad (2)$$

$$CH_4 + 0.5O_2 \leftrightarrow 2H_2 + CO \quad (POM) \quad (3)$$

POM is an exothermic reaction, while the SRM and DRM reactions are both endothermic. The H_2/CO ratio has a remarkable impact on the application of syngas. The H_2/CO ratio of syngas formed in DRM is usually less than one because of the high tendency of the Reverse Water Gas Shift (RWGS) [9-10].

The SRM reaction leads to producing the syngas with a larger H_2/CO ratio (higher than 3), which is not suitable to produce syngas for GTL process [14]. However, the syngas has been producing from SRM reaction is economical [7-8]. The products of POM are H_2 and CO with a ratio of about 2, which is preferred as feed for the FTS reaction. Nevertheless, POM reaction shows some drawbacks such as explosion danger and difficult operation controlling that have far-reaching consequences for pragmatic applications in the industry [11-13].

One suitable alternative to form syngas with a flexible H_2/CO ratio can be the combination of two SRM and DRM reactions as CSCRM reactions [15-33]. CSCRM has a remarkable advantage to producing syngas with various H_2/CO ratios using the adjusted H_2O/CO_2 ratio in the inlet feed [17]. Besides, side reactions including Methane Decomposition (MD), Water-Gas Shift (WGS), Reverse Water-Gas Shift (RWGS), and Boudouard reaction could be happened followed by CSCRM [17, 24], which are as follow:

$$CO + H_2O \leftrightarrow CO_2 + H_2 \quad (WGS \text{ and } RWGS) \quad (4)$$

$$CH_4 \leftrightarrow C + 2H_2 \quad (MD) \quad (5)$$

$$2CO \leftrightarrow C + CO_2 \quad (Boudouard\ reaction) \quad (6)$$

Nickel is often employed as an active metal in CSCRM reactions because of its low price, suitable catalytic performance, and good availability [26-27]. However, nickel-based catalysts suffer from severe coke formation, which intensifies the deactivation of catalyst [29-31]. Numerous scientists attempted to improve the catalytic activity and decrease the coke deposition by utilizing noble metals [26-27]. However, noble metals including Pt, Pd, Rh, Ru, etc have higher catalytic activity compared to Ni-based catalysts in the CSCRM reaction, but their applications are constrained due to the high cost and are frequently employed as a promoter [26-28]. *Batebi et al.* [26] perceived that methane conversion enhanced near 20% by adding Pd as a promoter to Ni/Al_2O_3 catalyst in the temperature range of 773 K-1273 K, while the amount of coke deposition was strikingly reduced especially at higher temperatures.

It is clear that support has a critical role in the catalyst activity, selectivity, and stability [15-16]. Al_2O_3, MgO, SiO_2, CeO_2, La_2O_3, ZSM-5, and SiO_2 supports are extensively studied in the CSCRM reaction [15-18, 22-28]. In the recent decade, numerous studies on Ni-based catalysts with bimodal pore structure supports were investigated in the literature [15-19, 27-29]. The performance of $Ni/MgO\text{-}Al_2O_3$ catalysts in CSCRM reaction was evaluated by *Koo et al.* [18]. Their outcomes illustrated the $Ni/MgO\text{-}Al_2O_3$ catalyst with Mg/Al ratio of 0.5 which presented a fine catalytic activity as well as high stability to the catalyst deactivation. *Dan et al.* [31] synthesized Ni/Al_2O_3, $Ni/La_2O_3\text{-}Al_2O_3$, and $Ni/MgO\text{-}Al_2O_3$ with a bimodal pore structure were prepared. Their results showed that Ni/Al_2O_3 catalysts promoted using MgO and La_2O_3 presented better structural and functional properties, also $Ni/La_2O_3\text{-}Al_2O_3$ catalyst had the best activity and stability among the catalysts [31]. *Yu et al.* [30] synthesized $Ni/MgAl_2O_4$ catalysts with different preparation methods and concluded that 10% $Ni/MgAl_2O_4$ catalyst synthesized using the sol-gel demonstrated better catalytic performance because of a strong interaction between active metal and support.

ZrO_2 a metal oxide with a great ion exchange performance and a surface enriched with oxygen vacancies has been remarkably employed as a support for GTL process [5]. The addition of zirconia to $Co\text{-}Pt/Al_2O_3$ catalyst in CSCRM reaction revealed a noticeable improvement in methane conversion and catalyst stability against coke deposition [15]. *Roh et al.* [22] prepared the $Ni/CeZrO_2$ catalysts with various Ce/Zr ratios and their results proved that $Ni/Ce_{0.8}Zr_{0.2}O_2$ had the maximum activity and stability in CSCRM reaction because of the NiO higher dispersion and nano-structure nature of $Ce_{0.8}Zr_{0.2}O_2$. The catalysts supported on ZrO_2 were synthesized *via* the co-precipitation method and NaOH as a precipitant exhibited superior performance in GTL process [5].

According to the above-mentioned studies, CSCRM reaction mostly focused on the influence of support with bimodal pore structure and promoter on the catalytic performance and stability against deactivation [15-16, 18-26, 28-33]. It should be noted that investigating the influence of operating variables on CSCRM reaction performance was only limited to the work of *Jang et al.* [17]. The influence of CO_2: H_2O ratio (in the range of 0.9-2.9), $(CO_2+H_2O)/CH_4$ ratio (in the range of 0.9-2.9) and pressure (1-20 bar) on the performance of Ni/MgO-CeO_2 catalyst was investigated in the CSCRM process [17]. It is reported that the H_2/CO ratio in the formed syngas was modified by altering the H_2O/CO_2 ratio in reaction feed, $(CO_2+H_2O)/CH_4$ ratio, and the process pressure [17]. The $(CO_2+H_2O)/CH_4$ ratio of 1.2 is the minimum requirement to avoid coke deposition and also when the H_2O/CO_2 ratio is greater than 2, a preferable H_2/CO ratio for GTL process can be obtained above 1120 K. Recently, the CSCRM reaction kinetic model was derived based on Langmuir–Hinshelwood approach and results showed the proposed mechanism error in predicting the responses was 8.52% [17].

In the present work, Ni/ZrO_2 catalyst was synthesized by the co-precipitation method. Then its physicochemical properties were examined *via* temperature-programmed Reduction (TPR), X-Ray Fluorescence (XRF), X-Ray Diffraction (XRD), N_2 adsorption/desorption (BET), Scanning Electron Microscope (SEM), and Temperature Programmed oxidation (TPO) tests, which has not been reported yet. The influence of temperature in the range of 773 K-1273 K, CO_2:H_2O ratio in the range of 0.5-3, and $(CO_2+H_2O)/CH_4$ ratio in the range of 0.5-3 variables on the CH_4 and CO_2 conversions, H_2 and CO yield, H_2/CO ratio and amount of coke formation on the catalyst surface in CSCRM reaction was evaluated to achieve the preferable operating conditions for GTL process.

EXPERIMENTAL SECTION

Preparation of Ni/ZrO_2 catalyst

The Ni/ZrO_2 nano-structure catalyst was synthesized via a co-precipitation approach in the presence of NaOH as a precipitant. A specified amount of nickel (II) nitrate hexahydrate ($Ni(NO_3)_2{\cdot}6H_2O$) and zirconium (IV) nitrate pentahydrate ($Zr(NO_3)_4{\cdot}5H_2O$) were dissolved in 50 mL of deionized water. Another 1 molar solution was obtained by dissolving a specified amount of NaOH in 25 mL of deionized water. The above two solutions were added to a round-bottomed flask containing 90 mL deionized water at 313 K under stirring, simultaneously. Then, the pH value was adjusted to 13, aged for 12 h at room temperature. The obtained sample was filtered and washed with deionized water several times. Each sample was dried at 373 K in vacuum condition for 10 h and calcined at 873 K for 5 h [34].

Catalyst characterization

The phase recognition was evaluated by an X-ray diffractometer (Shimadzu Company) with Cu Kα radiation. To identify the actual content of nickel elements in the synthesized sample, XRF analysis was carried out via a Bruker S4 Explorer spectrometer (Germany). The reduction behavior of the synthesized sample was examined by TPR analysis using a chemisorptions analyzer (Micromeritics, 2920). The catalyst treatment was performed via argon stream at a temperature 520 K for 2 h, and then the temperature was raised to 900 K to remove the humidity. Afterward, the reactor temperature was decreased to 293 K via a nitrogen gas stream. Finally, the catalyst was heated up to 1000 K with a 15 K/min ramp using a hydrogen gas stream. The surface area and porosity of ZrO_2 support and calcined catalyst were measured via BET analysis via a Quantachrome Nova 4200 apparatus. The morphology of the prepared catalyst was evaluated via the SEM analysis using Hitachi SU3500 apparatus.

The amount of carbon that was deposited on the spent catalysts was examined via temperature-programmed oxidation (TPO) test by ChemiSorb 2750 (Micrometrics Company). The spent catalysts were gathered after a long-term stability test for 150 h. First, the catalyst was loaded in a reactor and then situated in a furnace where the temperature was heated up to 950 K via a nitrogen stream for 2 h to eliminate the adsorbed gases and humidity. Afterward, the catalyst was reheated up to 1273 K *via* a mixture of oxygen and helium at a rate of 10 K/min. Also, the reactor outlet gases were examined via a Varian CP-3800 gas chromatograph.

Catalyst activity testing

Fig. 1 displayed a schematic diagram for the CSCRM experimental setup. The setup of CSCRM process included three sections: inlet feed, reactor, and products analyzer. Liquid water was vaporized through an evaporator

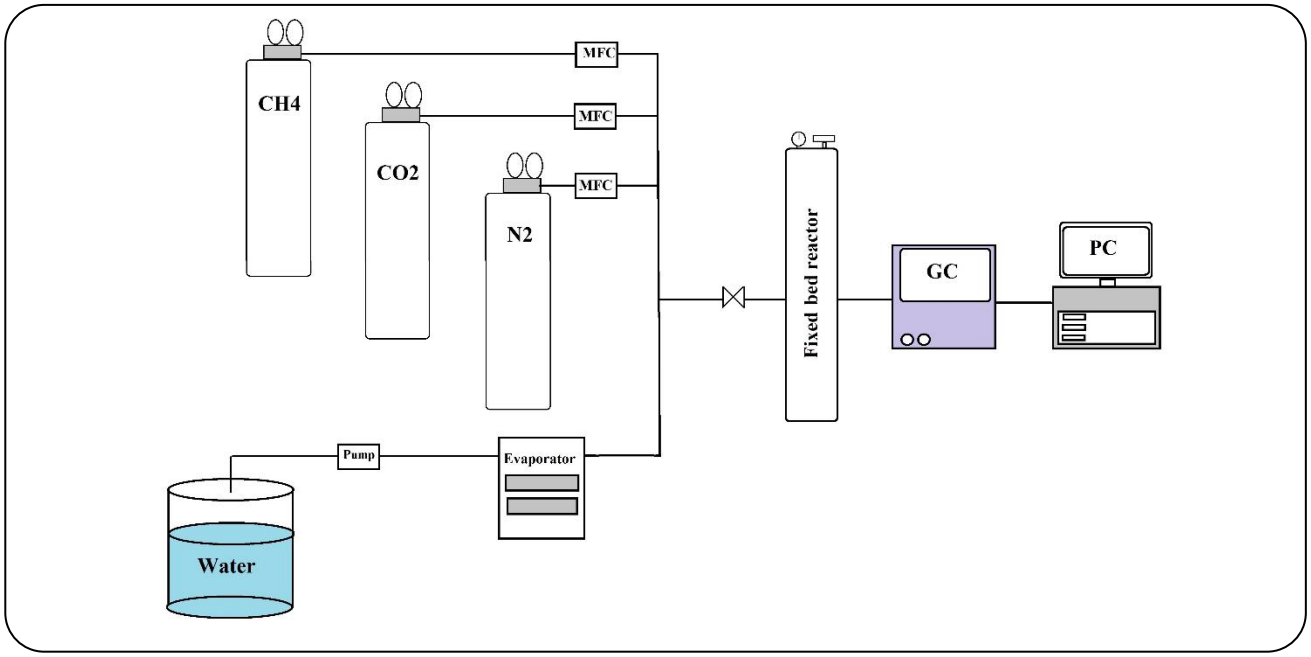

Fig. 1: The schematic diagram of the experimental setup.

and a piston pump was applied to control the liquid water flow rate. Generated steam was mixed with methane and carbon dioxide as reaction feed before entering the reactor. The flow rates of gas species were controlled *via* the mass flow controllers of Brooks. CSCRM tests were performed in a fixed bed reactor with lengths and diameters of 800 mm and 13 mm, respectively. The reactor was placed in a furnace with three separate controllers to measure the temperature of three reactor sections. Samples were situated in the center of the reactor. Before starting the process, the reduction treatment of catalysts was performed via hydrogen with Gas Hourly Space Velocity (GHSV) of 1300 1/h for 4 h at 1010 K, based on the results of temperature-programmed reduction analysis. The CSCRM process was performed at varied working conditions in the range of 773-1273 K, $(CO_2 + H_2O)/CH_4$ ratio of 0.5-3, CO_2:H_2O ratio of 0.5-3, GHSV of 1300 1/h and atmospheric pressure. Each CSCRM test was performed for 10 h. The outlet gases were examined *via* a Varian CP-3800 gas chromatograph.

To evaluate the performance of synthesized catalysts in CSCRM process, methane conversion (x_{CH4}) and products selectivity were measured as below:

$$2x_{CH_4}(\%) = \frac{\text{mole of the inlet methane} - \text{mole of the outlet methane}}{\text{mole of the inlet methane}} \times 100 \quad (7)$$

$$x_{CO_2}(\%) = \frac{\text{mole of the inlet } CO_2 - \text{mole of the outlet } CO_2}{\text{mole of the inlet } CO_2} \times 100 \quad (8)$$

$$CO\ Yield\ (\%) = \frac{\text{moles of the produced CO}}{(\text{moles of the inlet methane}) + (\text{mole of the inlet } CO_2)} \times 100 \quad (9)$$

$$H_2\ Yield\ (\%) = \frac{\text{moles of the produced } H_2}{2 \times (\text{mole of the inlet } CH_4) + (\text{mole of the inlet } H_2O)} \times 100 \quad (10)$$

RESULTS AND DISCUSSION

Effect of $(CO_2+H_2O)/CH_4$ ratio on the CSCRM reaction catalytic activity

Fig. 2a–e displayed the influences of $(CO_2 + H_2O)/CH_4$ ratio and temperature on the methane conversion, CO_2 conversion, H_2/CO ratio, H_2 and CO yield in the CSCRM process at a CO_2:H_2O ratio of 0.5. As can be seen in Fig. 2a, the higher $(CO_2+ H_2O)/CH_4$ ratios showed higher methane conversion as the temperature was above 973 K. The result revealed the insufficient amount of oxidizing agent as a limiting reactant led to lower CH_4 conversion [17].

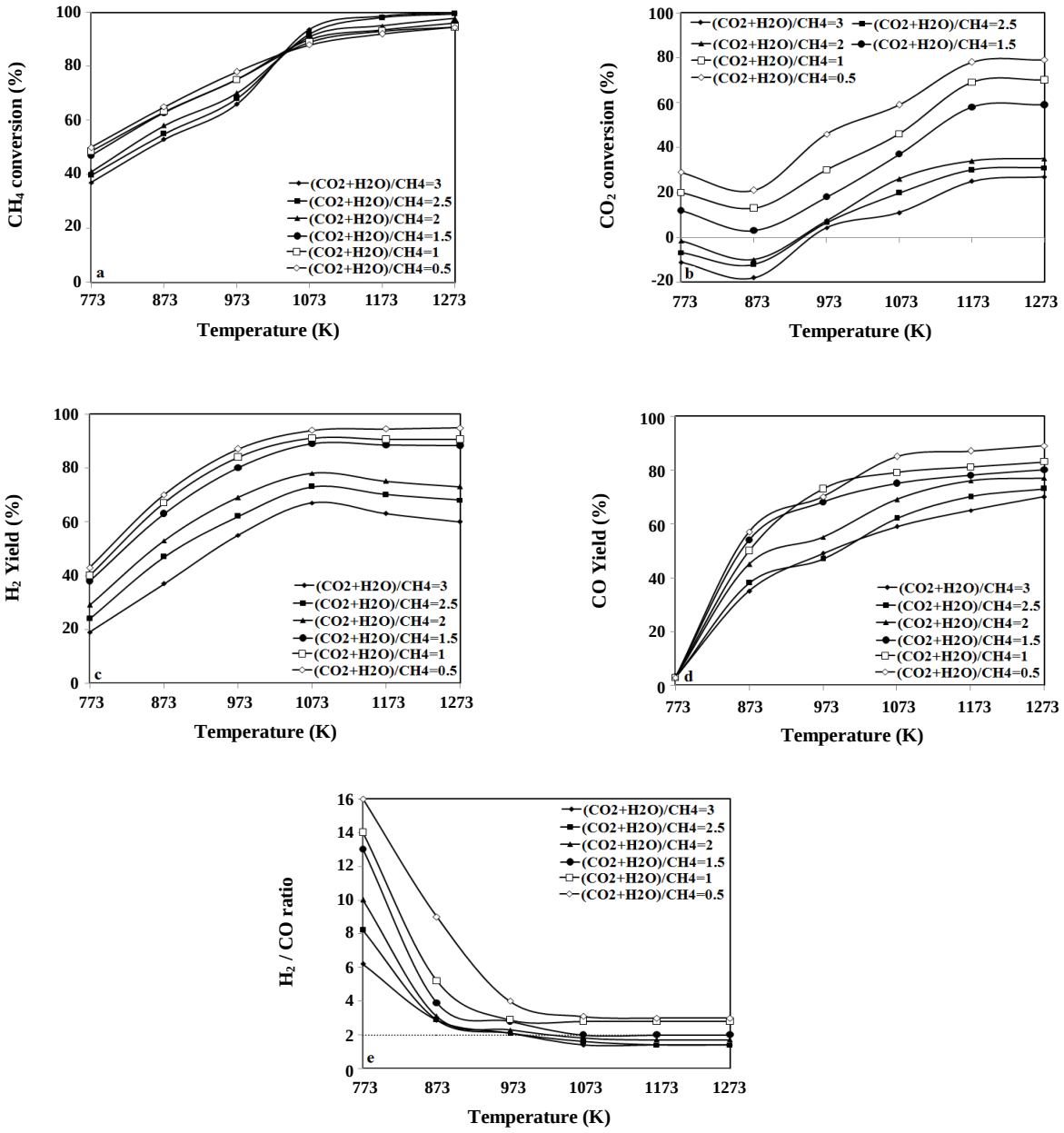

Fig. 2: The effects of (CO_2 + H_2O)/CH_4 ratio and temperature at a fixed CO_2:H_2O ratio of 0.5 on the (a) CH_4 conversion, (b) CO_2 conversion, (c) H_2 yield, (d) CO yield, and (e) H_2/CO ratio.

Nevertheless, the changes of CH_4 conversion versus (CO_2+ H_2O)/CH_4 ratio variable were exactly reversed below 973 K. It indicated that there was a great mutual dependency of temperature and (CO_2+H_2O)/CH_4 for CH_4 conversion. Thus, the CH_4 conversion of about 100% was achieved at (CO_2 + H_2O)/CH_4 ratio higher than 2 in the range of 1073 K-1273 K. *Jang et al.* [17] illustrated that except the (CO_2 + H_2O)/CH_4 ratio of 0.9, the CH_4 conversion reaches to 100% at a temperature higher than 1123 K. They stated that inadequate amount of oxidizing agent results in the low methane conversion since the oxidizing agent was presumed as the limiting reactant.

Fig. 2b indicates the CO_2 conversion trends as a function of temperature for different (CO_2 + H_2O)/CH_4 ratios at a fixed CO_2:H_2O ratio of 0.5. The CO_2 conversion remarkably decreased when the (CO_2 + H_2O)/CH_4 ratio

increases from 0.5 to 3. These results exhibited that the $(CO_2+H_2O)/CH_4$ ratio has a greater influence on the CO_2 conversion than CH_4 conversion. CO_2 conversion was augmented by increasing the temperature in the range of 873 K-1173 K, while this trend was reversed below 873 K. *Özkara-Aydinoğ lu* [32] observed that CO_2 conversion has a negative value for higher $(CO_2 + H_2O)/CH_4$ ratios in the range of 773 K-873 K, which agreed well with the outcomes of our study. According to Eq. 4, the CO and H_2O are transformed into H_2 and CO_2 in WGS reaction so that the produced CO_2 via WGS reaction was greater compared to the consumed CO_2 via DRM at lower temperatures [7, 26]. It is evident that the effect of reaction temperature on the CO_2 conversion was not significant in the temperature range of 1173 K-1273 K (see Fig. 2b). *Jang et al.* [17] monitored a similar trend for $(CO_2 + H_2O)/CH_4$ ratios of (i.e., 0.9, 1.2 and 1.4). Nevertheless, they observed that for higher $(CO_2 + H_2O)/CH_4$ ratios of 2.0 and 2.9, H_2 yield started decreasing at 1073 K. They demonstrated that this phenomenon can be because of the RWGS occurrence. Thus, it led to the consumption of H_2 by RWGS (Eq. (4)), and finally, the H_2 yield was reduced at temperatures above 1073 K [26].

Fig. 2c exhibited H_2 yield in terms of temperature with different $(CO_2 + H_2O)/CH_4$ ratios. It is obvious that the H_2 yield has increased by the reduction of $(CO_2 + H_2O)/CH_4$ ratio in the range of 0.5 to 3. This can be related to the excess CO_2 with produced H_2 which is converted to CO and H_2O by RWGS and consequently results in the lower H_2 yield at a higher $(CO_2 + H_2O)/CH_4$ ratio. At $(CO_2 + H_2O)/CH_4$ ratios of 0.5, 1, 1.5, H_2 yield almost was constant in the range of 1073 K-1273 K, while H_2 yield decreased for $(CO_2 + H_2O)/CH_4$ ratios of 2, 2.5, and 3. Our previous work proved the RWGS reaction was favorable compared to the WGS at temperatures higher than 1073 K [32] so that the excess CO_2 reacted with H_2 and the value of consumed H_2 in RWGS was higher than produced H_2 in SRM.

The changes in CO yield versus temperature with various $(CO_2 + H_2O)/CH_4$ ratio has been depicted in Fig. 2d. It is clear that the CO yield at the lower $(CO_2 + H_2O)/CH_4$ ratios (i.e., 0.5, 1 and 1.5 was higher compared to $(CO_2 + H_2O)/CH_4$ ratios of 2, 2.5 and 3. According to Fig. 2c and d, the H_2 yield was higher than CO yield under identical operating conditions. Also, the CO yield was increased by the rising temperature in the range of 773 K-1273 K. This proved that SRM and DRM reactions were favorable at a higher temperature.

Additionally, the variation of H_2/CO ratio in terms of temperature for various $(CO_2 + H_2O)/CH_4$ ratios is demonstrated in Fig. 2e. The values of high H_2/CO ratios were achieved at temperatures lower than 873 K. This was because of the hydrogen produced via the MD (Eq. 5) and the CO consumed via the Boudouard reaction (Eq. 6) and WGS (Eq. 5) [17]. H_2/CO ratio gently reached a range of 1.4-3 by increasing the temperature. For $(CO_2 + H_2O)/CH_4$ ratios of 0.5 and 1, H_2/CO ratio reached 2.4 in the range of 1073 K - 1273 K. At lower $(CO_2 + H_2O)/CH_4$ ratios, excess methane can be converted to coke and hydrogen without producing carbon monoxide via MD reaction [32]. At $(CO_2 + H_2O)/CH_4$ ratio of 1.5, H_2/CO ratio gradually approached near 2 at temperatures higher than 1073 K, which was appropriate for FTS reaction. For $(CO_2 + H_2O)/CH_4$ ratios of 2, 2.5, and 3, H_2/CO ratio was higher than 2.0 between 973 K-1073 K, as SRM reaction was prevailing compared to the DRM. H_2/CO ratio decreased to lower than 2 (in the range of 1.4-1.7) above 1073 K. This might be probably attributed to the favorability of the DRM and RWGS reactions over the SRM at a temperature higher than 1073 K [17, 32]

Effect of CO_2:H_2O ratio on the CSCRM reaction catalytic activity

Fig. 3a–e presented the influences of the CO_2:H_2O ratio and temperature on methane conversion, CO_2 conversion, H_2/CO ratio, H_2 and CO yield in the CSCRM reaction for $(CO_2 + H_2O)/CH_4$ ratio of 1.5. Due to the H_2/CO ratio obtained at about 2 at $(CO_2 + H_2O)/CH_4$ ratio of 1.5, this value was selected for further experiments. According to Fig. 3a, methane conversion has been greatly augmented by rising the temperature that can be assigned to the endothermic nature of the SRM and DRM reactions [7]. The methane conversion increased by raising the CO_2:H_2O ratio in the range of 0.5 to 3 (see Fig. 3a). When the portion of carbon dioxide was greater compared to the steam in the inlet feed, a noticeable amount of methane converted at a temperature lower than 973 K. Although, methane conversion did not change against CO_2:H_2O ratios in the temperature range of 1073 K-1273 K. It should be noted that methane conversion reached near 100 % at a temperature above 1173 K in all values of CO_2:H_2O ratios.

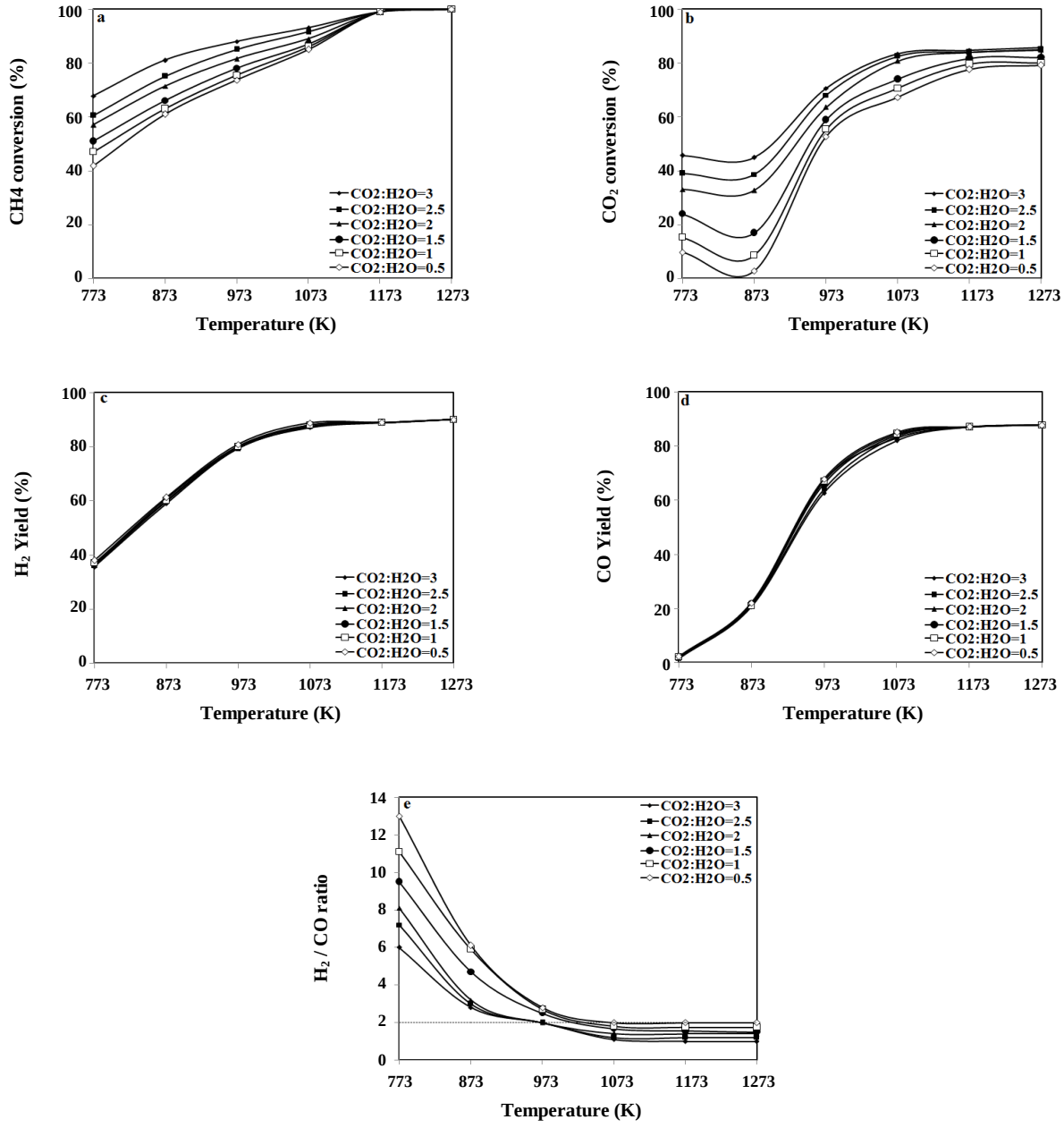

Fig. 3: The effects of the CO_2:H_2O ratio and temperature at a fixed (CO_2 + H_2O)/CH_4 ratio of 1.5 on the (a) CH_4 conversion, (b) CO_2 conversion, (c) H_2 yield, (d) CO yield, and (e) H_2/CO ratio.

Fig. 3b exhibited the CO_2 conversion in terms of the temperature with different CO_2:H_2O ratios. As depicted in Fig. 3b, CO_2 conversion has increased as the CO_2:H_2O ratio increases. The increase of CO_2 portion in oxidizing agent caused the DRM reaction to become more desirable than the SRM reaction [7, 26], thereby the CO_2 conversion increased.

CO_2 conversion for CO_2:H_2O ratios of 0.5, 1, and 1.5 decreased with increasing temperature, while CO_2 conversion for CO_2:H_2O ratios of 2, 2.5, and 3 remained relatively unchanged in the range of 773 K-873 K. This indicated to the rate of CO_2 consumption *via* DRM is almost the same with CO_2 produced *via* WGS in the range of 773 K-873 K. Similar to Fig. 2b, the CO_2 conversion increased by increasing of temperature at 873 K-1173 K. This expressed that DRM (due to its highly endothermic nature) and RWGS were predominant reactions at higher

temperatures [7, 17, 26]. For CO_2:H_2O ratios of 2, 2.5, and 3, the trends of CO_2 conversion against temperature overlapped in the range of 1173 K-1273 K. For all CO_2:H_2O ratios, CO_2 conversion values were close to each other in the range of 1173 K- 1273 K.

H_2 and CO yields in terms of the temperature at different CO_2:H_2O ratios are presented in Fig. 3c and d. As can be seen, the changes in H_2 and CO yields with CO_2:H_2O ratios were little. This indicated that the same portion of reactants can be transformed into hydrogen and carbon monoxide, even at the various CO_2:H_2O ratios. Comparing Fig. 2c and d with Fig. 3c and d, it can be concluded that the yield of the syngas formation was completely independent of CO_2:H_2O ratio, while affected by (CO_2 + H_2O)/CH_4 ratio. These results were in perfect harmony with the study of *Jang et al.* [17]. Furthermore, H_2 yield was increased by soaring temperature in the range of 773 K– 1073 K. This affirms that H_2 was produced by SRM, DRM, and WGS reactions. It is obvious that the changes in H_2 yield with temperature were not noticeable in the range of 1073 K – 1273 K (see Fig. 3c). This indicated that H_2 produced by SRM and DRM reactions is almost similar to hydrogen consumed in RWGS. The CO yield is significantly augmented by raising the temperature owing to the preferable nature of reforming reactions at high temperatures [32]. Below 1073 K, the ascending trend of CO yield in terms of temperature was intensive, whereas, for temperatures above 1073 K, the trend gradually increased. Although, the influence of temperature on the CO yield was greater compared to H_2 yield.

Fig. 3e depicted the changes in H_2/CO ratio against temperature at various CO_2:H_2O ratios. When the portion of CO_2 was greater compared to steam, syngas with a low H_2/CO ratio (lower than 2) was produced using the DRM reaction [17]. The H_2/CO ratio was augmented by raising the steam amount in the reaction feed because of the occurrence of SRM. Thereby, it was demonstrated that H_2/CO ratio in formed syngas can be controlled by altering the CO_2:H_2O ratio at a constant (CO_2 + H_2O)/CH_4 ratio. For CO_2:H_2O ratios of 3, 2.5, 2, 1.5, and 1, the H_2/CO ratio was more than 2 at below 973 K, while this value was lower than 2 at above 973 K. For CO_2:H_2O ratio of 0.5, H_2/CO ratio declined from 13 to 2 in the range of 773 K-1073 K. In addition, to produce the syngas with the H_2/CO ratio of 2 (suitable for GTL process), the CO_2:H_2O ratio and temperature should be 0.5 and above 1073 K, respectively. The H_2/CO ratio reached a constant value by raising the temperature in the range of 1073 K– 1273 K. The decrease in H_2/CO ratio at higher temperatures can be related to the DRM reaction being favorable compared to the SRM [17]. Conversely, the H_2/CO ratio decreased to lower than 2 at temperatures above 1173 K for (CO_2 + H_2O)/CH_4 ratios of 2 and 2.9 [17, 32].

TPO analysis

Fig. 4a demonstrated the amount of deposited coke on the catalyst surface obtained via TPO analysis in terms of temperature for various (CO_2 + H_2O)/CH_4 ratios at CO_2:H_2O ratio of 0.5.

The amount of coke decreased by raising the (CO_2 + H_2O)/CH_4 ratio. This proved that the higher (CO_2 + H_2O)/CH_4 ratio can decrease the coke deposition. For the (CO_2 + H_2O)/CH_4 ratios (i.e., 3, 2.5, 2, and 1.5), coke formation was about zero at above 1073 K. The above results revealed that higher temperature and (CO_2 + H_2O)/CH_4 ratio avoid the coke formation. For the (CO_2 + H_2O)/CH_4 ratios of 1.2 and 1.4, the amount of coke deposition reached almost zero when the temperature increased up to 1023 K. The coke deposition on this catalyst is attributed to the MD reaction (Eq.(5)) and the Boudouard reaction (Eq. (6)) [17, 26]. *Ruckenstein* and *Wang* [35] comprehended that catalyst deactivation in DRM reaction was because of both coke formation and oxidation of metallic sites. They declared that the stability of Co/Al_2O_3 catalysts in DRM reaction was strikingly affected by the cobalt content and the calcination temperature. It should be determined the temperature dependence of carbon-containing products in the MD and Boudouard reactions, separately. The amounts of carbon-containing products versus temperature were listed in Table 1. However, the MD was desirable at high temperatures, but a noticeable amount of coke deposition was seen at low temperatures.

The Boudouard reaction was suitable at low temperatures and did not happen above 1073 K. This indicated that the coke formation is because of both the Boudouard and MD reactions, but the portion of the Boudouard reaction is higher at low temperatures. While the portion of MD in the coke deposition expanded by increasing the temperature. Therefore, the main factors of

Table 1: Carbon containing product for the various reactions.

Reaction	Temperature (K)	Carbon containing product (%)			
		CH_4	C	CO_2	CO
MD (CH_4=100 %)	773	62	38	---	---
	873	33.12	66.76	---	---
	973	17.34	82.66	---	---
	1073	4.78	95.22	---	---
	1173	2.23	97.77	---	---
	1273	1.11	98.89	---	---
Boudouard (CO=100%)	773	---	51.12	42.18	6.6
	873	---	40.15	42.34	17.51
	973	---	22.65	17.3	60.05
	1073	---	6.43	6.28	87.29
	1173	---	2.13	---	97.87
	1273	---	1.56	---	98.44
SRM (CH_4:H_2O=1)	773	57.12	20.07	15.28	7.53
	873	32.12	27.89	12.76	27.23
	973	13.23	12.55	6.13	68.09
	1073	4.98	2.22	2.06	90.74
	1173	1.87	0.97	---	97.16
	1273	1.05	---	---	98.95
DRM (CH_4:CO_2=1)	773	8.04	56.47	31.24	4.25
	873	5.12	42.43	21.58	30.87
	973	3.35	21.79	11.38	63.48
	1073	1.76	6.22	5.12	86.9
	1173	---	3.03	1.35	95.62
	1273	---	0.96	---	99.04

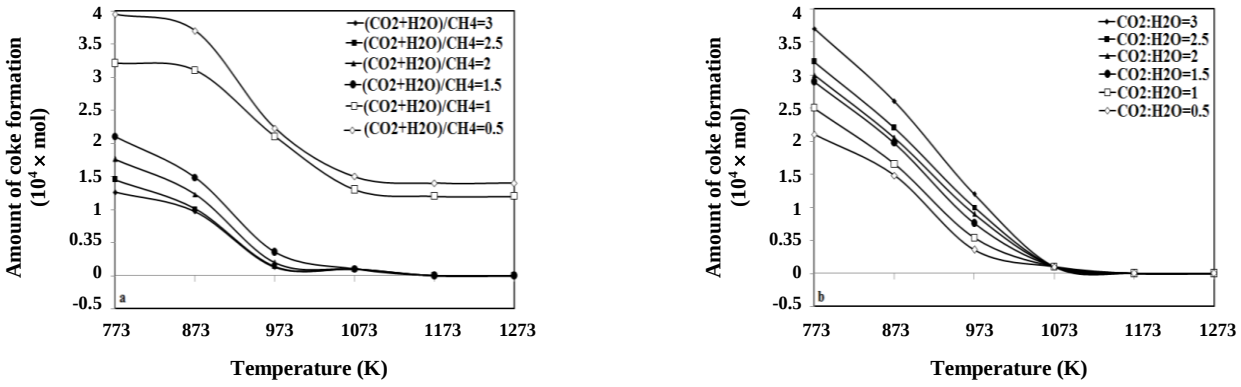

Fig. 4: Amount of coke deposition in terms of (a) (CO_2 + H_2O)/CH_4 ratio and temperature at a fixed CO_2:H_2O ratio of 0.5, (b) CO_2:H_2O ratio, and temperature at a fixed (CO_2 + H_2O)/CH_4 ratio of 1.5.

coke deposition was MD and Boudouard reactions at (CO_2 + H_2O)/CH_4 ratios of 0.5 and 1. The amount of coke was near zero for (CO_2 + H_2O)/CH_4 ratios of 1.5, 2, 2.5, and 3 above 1073 K irrespective of the CO_2: H_2O ratio.

Fig. 4b showed the amount of accumulated coke in terms of CO_2:H_2O ratio at (CO_2 + H_2O)/CH_4 ratios of 1.5. When the portion of carbon dioxide was larger than that of steam in the inlet feed, the coke formation was intensified below 1073 K. It was proved that the temperature, type, and amount of the oxidizing agent had a remarkable effect on the coke formation [17, 27, 32]. This described that even if the portion of oxidizing agents and methane was the same in the reaction feed, the coke formation strikingly depends on the type of oxidizing agent [17].

The influence of the type of oxidizing agent on the carbon-containing products, reactions of SRM (CH_4 = 50% and H_2O = 50%) and DRM (CH_4 = 50% and CO_2 = 50%) were accomplished individually, which outcomes are displayed in Table 1. It is clear that the CO_2 had a higher portion than H_2O in the coke formation. Thereby, the steam can remarkably prevent coke formation compared to carbon dioxide, which was entirely compatible with the results of Fig. 4b. However, it should be noted that the amount of coke deposition was very little above 1073 K for both SRM and DRM reactions. Above 1073 K, the large quantity of the carbon-containing agent was CO for both SRM and DRM reactions, and also there were no CH_4 and CO_2.

Generally, three variables of temperature, type, and amount of the oxidizing agent can be affected by the coke deposition. Below 1073 K, the coke deposition was implied on the type and amount of the oxidizing agent. However, above 1073 K, the (CO_2 + H_2O)/CH_4 ratio (amount of the oxidizing agent) had a powerful influence on the coke formation**.**

TPR analysis

TPR test was performed to evaluate the reducibility of the catalyst synthesized by the precipitation method, and the reduction spectrum was displayed in Fig. 5. The two reduction peaks were seen in the TPR profile of Ni/ZrO_2 catalyst. The low-temperature reduction peak occurred at around 630 K, which can be related to the reduction of bulk NiO species to metallic nickel [30]. The high-temperature peak at around 720 K corresponded to the reduction of NiO species which interacted with ZrO_2

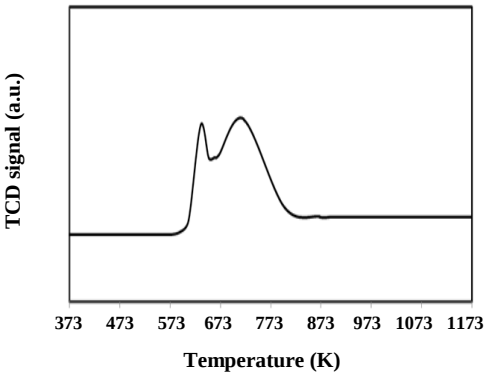

Fig. 5: TPR spectrum of the calcined catalyst.

support [36]. In the literature [34], two hydrogen consumption peaks with different areas occurred in the range of 573 K-823 K for Ni/ZrO_2 catalyst prepared by the impregnation method. They demonstrated that the low-temperature peak might be implied by the reduction of nickel oxide which weakly interacts with ZrO_2, and the high-temperature peak showed the existence of NiO species that strongly interact with ZrO_2 [34]. However, Ni/ZrO_2 catalyst synthesized by combustion method only had one H_2 reduction peak at 800 K that indicating a strong interaction between nickel oxide species with the support [34, 36].

XRF analysis

The physicochemical properties of the synthesized sample are illustrated in Table 2. The XRF analysis proved that nickel's actual content was 9.89 wt%. According to XRF outcomes, the actual content was near the nominal value (10 wt %). Although, the actual loading was much lower than its nominal value. This would be related to the segment of nickel species decomposed during the calcination treatment.

XRD analysis

The XRD spectrum of the Ni/ZrO_2 catalyst was seen in Fig. 6. According to Fig. 6a, the diffraction peaks at 2θ angle of 30. 3°, 50.6°, and 60.32° can be indexed to the (1 1 1), (2 2 0), and (3 1 1) tetragonal ZrO_2 [JCPDS No.79-1771], and the typical peaks at 24.1° and 28.1° related to ZrO_2 crystal phase with monoclinic structure [JCPDS 37-1484]. After the reduction treatment, it was clear that the intensity of monoclinic ZrO_2 peaks

was decreased, while the peaks intensity of the tetragonal phase was increased (see Fig. 6b). It is generally reported that ZrO_2 phase started to change from monoclinic to tetragonal state when the reduction temperature was bigger than 1273 K [36]. The diffraction peaks appearing at 43.2° and 63.1° would correspond to NiO species in the calcined catalyst (see Fig. 6a) [7, 27, 34, 36]. The NiO species were not seen in the XRD spectrum of the reduced catalyst, which was proved nickel oxide entirely transformed to metallic nickel during the reduction treatment (see Fig. 6b).

The peaks were revealed at 44.1° and 76.3° attributed to the metallic nickel in the XRD profile of the reduced catalyst [JCPDS 04-0850]. The average nanoparticle size of nickel was measured *via* the Scherrer equation: $d = K\lambda/\beta \cos\theta$, where d is the particle size, K is a constant (K = 0.9), λ is the wavelength of X-ray (Cu Kα= 0.154 nm) and β is the width of the peak at half of the maximum height. The particle size of NiO and metallic nickel in the calcined and reduced catalysts were about 16 nm and 27 nm, respectively. This increment would be related to the Ni particle agglomeration during the reduction treatment, which is well agreed with various reports [27].

SEM analysis

SEM images of the Ni/ZrO_2 catalysts were seen in Fig. 7. It was clear that spherical shape nanoparticles were homogeneously distributed on the support external surface without remarkable sintering emerging before reduction treatment (see Fig. 7a). The particle size distribution histogram measured through SEM analysis and particles size was in the range of 7–32 nm with an average of 17 nm (see Fig. 8a).

The smaller particles aggregated to form a larger particle during the catalyst reduction treatment because of sintering (see Fig. 7b). For the reduced catalyst, the agglomeration of the nickel species was more prevalent than the unreduced catalyst. Thereby, the average particle size in the reduced catalyst was bigger compared to the unreduced catalyst. According to Fig. 8b, the particle size of the reduced catalyst was between 12-60 nm with an average size of 29 nm. The average particle size obtained by SEM analysis was near to the values measured using XRD test.

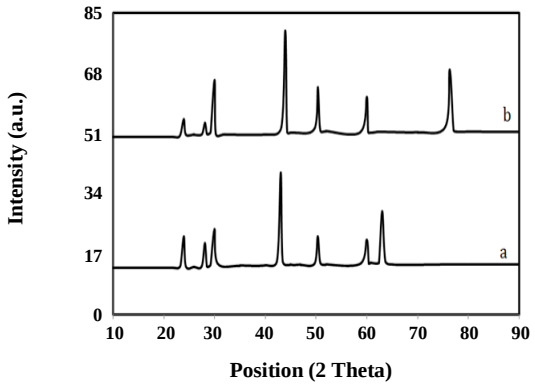

Fig. 6: The XRD patterns of (a) the calcined catalyst, (b) the reduced catalyst.

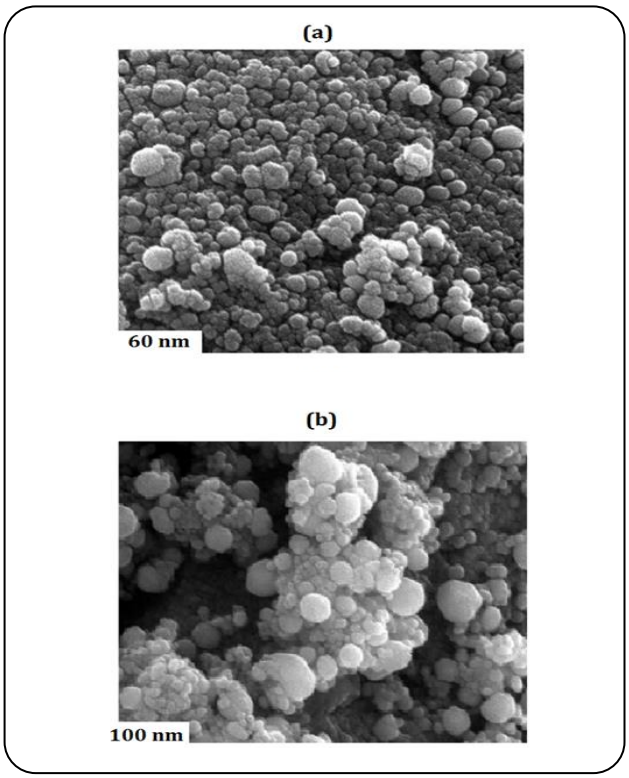

Fig. 7: The SEM images of (a) The calcined catalyst, (b) The reduced catalyst.

BET analysis

BET analysis was performed to examine the surface area, pore volume, and average pore size of the support and the prepared catalyst (see Table 2). The loading of nickel on the ZrO_2 support led to a decrease in the surface area from 221.24 m^2/g to 188.46 m^2/g (see Table 2). In addition, pore volume and average pore size of Ni/ZrO_2 catalyst were smaller than pure ZrO_2, which would be

Table 2: Physicochemical properties of Ni/ZrO_2 catalyst.

Catalyst	Ni (wt%)	Surface area (m^2/g)	Pore volume (cm^3/g)	Average pore size (nm)
ZrO_2	---	221.24	0.69	8.21
10% Ni/ZrO_2	9.89	188.46	0.55	6.87

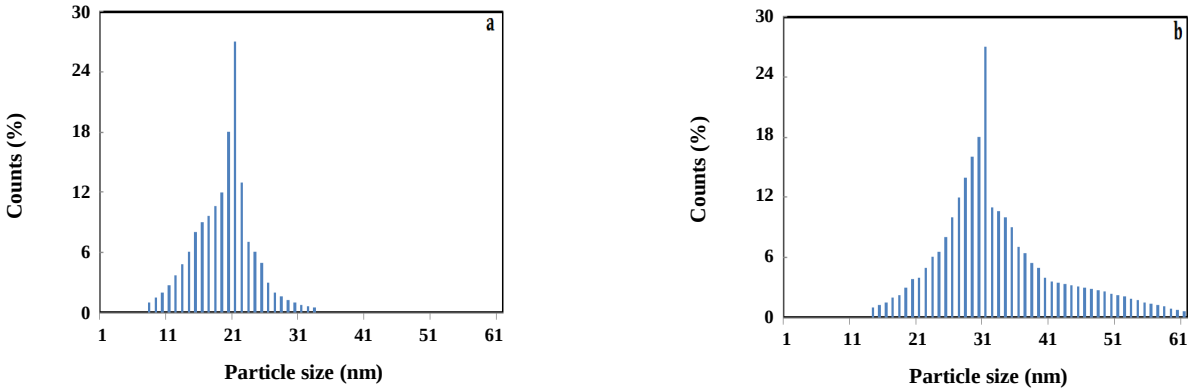

Fig. 8: The particle size distribution measured by SEM analysis for (a) the calcined catalyst, (b) the reduced catalyst.

due to the partial blockage of ZrO_2 pores during the sample synthesis [2-4].

The stability test

Fig. 9 showed the stability test of Ni/ZrO_2 catalyst in CSCRM reaction at different operating conditions. At temperature 1173 K, CO_2:H_2O ratio of 0.5 and (CO_2+H_2O)/CH_4 ratio of 1.5, methane conversion, H_2/CO ratio, H_2 and CO yields were almost unchanged during 150 h on stream. This indicated that the amount of coke formation on the catalyst surface was zero according to TPO analysis results.

Jang et al. [17] described that conversions and yields were stable and without any deactivation at 1123 K, CO_2:H_2O ratio of 0.5, and (CO_2+H_2O)/CH_4 ratio of 1.2.

At temperature 873 K, CO_2:H_2O ratio of 0.5 and (CO_2+H_2O)/CH_4 ratio of 0.5, methane conversion was extremely stable during 120 h initial on stream with 66.27%, and then started to decrease to 58.84% in the time period of 120 h to 150 h (see Fig. 9a). The catalyst deactivation in CSCRM reaction was because of the carbon deposition via Boudouard reaction according to TPO test results. The values of H_2 and CO yield were nearly fixed up to 110 h initial and then started to reduce between 110 h- 150 h (see Fig. 9b and c). However, the decreasing CO yield was higher compared to H_2 yield, which would be attributed to the Boudouard reaction occurrence and finally high consumption of carbon monoxide. It was apparent that H_2/CO ratio was unchanged at about 8.92 up to 110 h and then started to augment to 9.82 between 110 h - 150 h (see Fig. 9d). This growth related to the decrease in CO yield was bigger than H_2 yield.

CONCLUSIONS

The influence of (CO_2+H_2O)/CH_4 ratio, CO_2:H_2O ratio, and the process temperature on the performance of CSCRM in the presence of Ni/ZrO_2 catalyst was investigated. We achieved the most conversions in higher (CO_2 + H_2O)/CH_4 ratios and temperatures with the CO_2:H_2O ratio of 0.5. The higher values of CO_2 conversion, CO, and H_2 yield were attained at a lower (CO_2 + H_2O)/CH_4 ratios. It was found that the H_2/CO ratio, methane, and CO_2 conversions can be controlled by altering the CO_2:H_2O ratio.

However, changing the CO and H_2 yield with CO_2:H_2O ratio was little. At (CO_2 + H_2O)/CH_4 ratio of 1.5 and CO_2:H_2O ratio of 0.5, the H_2/CO ratio gradually approached approximately 2 at temperatures higher than 1073 K, this is preferable operating conditions for syngas preparation in the GTL process. The variables of temperature, type, and amount of the oxidizing agent significantly affected the coke deposition. The amount of coke deposition decreased by raising the (CO_2 + H_2O)/CH_4 ratio. Temperature above

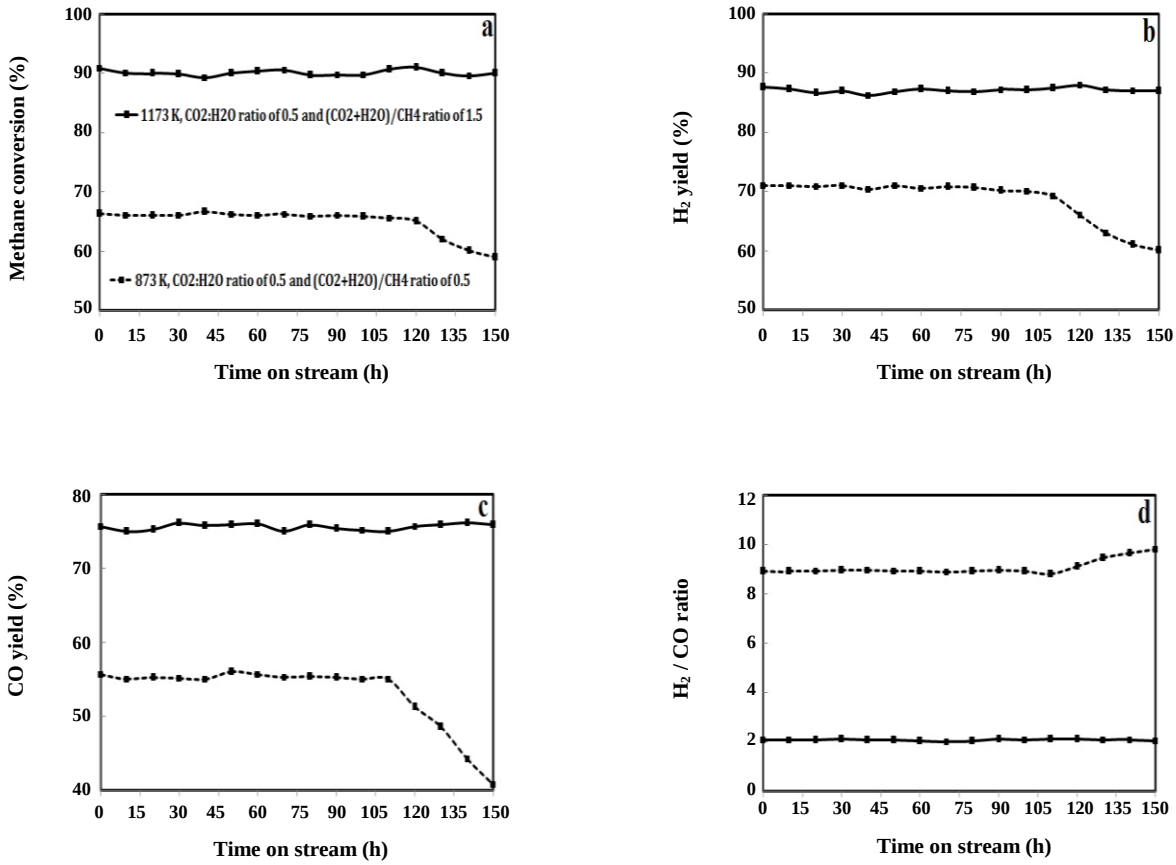

Fig. 9: The stability test of catalyst in CSCRM reaction at different operating conditions (a) methane conversion, (b) H_2 yield, (c) CO yield, and (d) H_2/CO ratio.

1073 K was required to avoid coke deposition except at the $(CO_2 + H_2O)/CH_4$ ratio of 0.5 and 1 irrespective of CO_2:H_2O ratio. However, the amount of coke deposition decreased by enhancing steam loading in the oxidizing agent.

Received : May. 4, 2021 ; Accepted : July 5, 2021

REFERENCES

[1] Fazeli SM., Bozorgzadeh H., Ravari F., Sadeghzadeh Ahari J., Dry Reforming of Methane Using Cold Plasma; Kinetic Model Study, *Iran. J. Chem. Chem. Eng. (IJCCE)*, **39**: 257-265 (2020).

[2] Mosayebi A., Abedini R., Effect of Synthesis Solution pH of Co/Al_2O_3 Catalyst on Its Catalytic Properties for Methane Conversion to Syngas, *J. Fuel. Chem. Technol.*, **46**: 311-318 (2018).

[3] Shariati J., Haghtalab A., Mosayebi A., Fischer–Tropsch Synthesis Using Co and Co-Ru Bifunctional Nanocatalyst Supported on Carbon Nanotube Prepared via Chemical Reduction Method, *J. Energy. Chem.*, **28**: 9-22 (2019).

[4] Haghtalab A., Shariati J., Mosayebi A., Experimental and Kinetic Modeling of Fischer–Tropsch Synthesis over Nano Structure Catalyst of Co–Ru/Carbon Nanotube, *React. Kinet. Mech.Catal.*, **126**: 1003-1226 (2019).

[5] Mosayebi A., Nasabi M., Abedini R., Evaluation and Modeling of Fischer-Tropsch Synthesis in Presence of a Co/ZrO_2 Catalyst, *Petrol. Sci. Technol.*, **37**: 2338-2349 (2019).

[6] Trépanier M., Tavasoli A., Anahid S., Dalai AK., Deactivation Behavior of Carbon Nanotubes Supported Cobalt Catalysts in Fischer-Tropsch Synthesis, *Iran. J. Chem. Chem. Eng. (IJCCE)*, **30**: 37-47 (2011).

[7] Mosayebi A., Nasabi M., Steam Methane Reforming on $LaNiO_3$ Perovskite Type Oxide for Syngas Production, Activity Tests, and Kinetic Modeling, *Int. J. Energy Res.*, **44**: 5500-5515 (2020).

[8] Nasabi M., Labbafi M., Hadinezhad M., Khanmohammadi M., Bagheri Garmarudi A., Investigation of TiO_2 Nanoparticle Efficiency on Decolourisation of Industrial Date Syrup, *Int. J. Food. Sci. Technol.*, **48**: 316-323 (2013).

[9] Habibi N., Wang Y., Arandiyan H., Rezaei M., Effect of Substitution by Ni in $MgAl_2O_4$ Spinel for Biogas Dry Reforming, *Int. J. Hydrogen. Energy.*, **42**: 24159-24168 (2017).

[10] Gao X., Tan Z., Hidajat K., Kawi S., Highly Reactive Ni-Co/SiO_2 Bimetallic Catalyst via Complexation with Oleylamine/Oleic Acid Organic Pair for Dry Reforming of Methane, *Catal. Today.*, **281**: 250-258 (2017).

[11] Mosayebi A., Kinetic Modeling of Catalytic Partial Oxidation of Methane over Ni-Rh/γ-Al_2O_3 Catalyst for Syngas Formation, *J. Taiwan. Inst. Chem. E.*, **114**: 36-46 (2020).

[12] Mosayebi A., Abedini R., Partial Oxidation of Butane To Syngas Using Nano-Structure Ni/zeolite Catalysts, *J. Ind. Eng. Chem.*, **20**:1542–1548 (2014).

[13] Shahnazari M.R., Lari H.R., Zia Basharhagh M., Simulation of Methane Partial Oxidation in Porous Media Reactor for Hydrogen Production, *Iran. J. Chem. Chem. Eng. (IJCCE)*, **38**: 201-212 (2019).

[14] fazeli S.M., Bozorgzadeh H.R., Ravari F., Sadeghzadeh Ahari J., Dry Reforming of Methane Using Cold Plasma; Kinetic Model Study, *Iran. J. Chem. Chem. Eng. (IJCCE)*, **39**: 257-265 (2020).

[15] Itkulova S.S., Nurmakanov Y.Y., Kussanova S.K., Boleubayev, B., Production of a Hydrogen-Enriched Syngas by Combined CO_2-Steam Reforming of Methane Over Co-Based Catalysts Supported on Alumina Modified With Zirconia, *Catal. Today.*, **299**: 272-279 (2018).

[16] Roh HS., Koo KY., Joshi UD., Yoon, WL., Combined H_2O and CO_2 Reforming of Methane Over Ni-Ce-ZrO_2 Catalysts for Gas to Liquids (GTL), *Catal. Letter.*, **125**: 283-288 (2008).

[17] Jang W.J., Jeong D.W., Shim J.O., Kim H.M., Roh H.S., Seung I.H., Lee, J., Combined Steam and Carbon Dioxide Reforming of Methane and Side Reactions: Thermodynamic Equilibrium Analysis and Experimental Application, *Appl. Energy.*, **173**: 80-91 (2016).

[18] Koo K.Y., Roh H.S., Jung U.H., Seo D.J., Seo Y.S., Yoon W.L., Combined H_2O and CO_2 reforming of CH_4 over Nano-Sized Ni/MgO-Al_2O_3 Catalysts for Synthesis Gas Production for Gas to Liquid (GTL): Effect of Mg/Al Mixed Ratio on Coke Formation, *Catal. Today.*, **146**:166–171(2009).

[19] Nasabi M., Labbafi M., Khanmohammadi M., Optimizing Nano TiO_2 Assisted Decoloration Process for Industrial Date Syrup Utilizing Response Surface Methodology, *J. Food. Process. Eng.*, **40**: e12537 (2017).

[20] Wei Q., Yang G., Gao, H., Yamane N., Zhang P., Liu, G., Ni/Silicalite-1 Coating Being Coated on SiC Foam: A Tailor-Made Monolith Catalyst for Syngas Production Using A Combined Methane Reforming Process, *Chem. Eng. J.*, **327**: 465-473 (2017).

[21] Mosayebi A., Methanol Steam Reforming over Co-Cu-Zn/Al_2O_3 Catalyst: Kinetic and RSM-BBD Modeling Approaches, *Int. J. Energy Res.*, **45**: 3288-3304 (2021).

[22] Roh H.S., Koo KY., Jeong J.H., Seo Y.T., Seo D.J., Seo Y.S., Combined Reforming of Methane over Supported Ni Catalysts, *Catal. Letter.*, **117**: 85–90 (2007).

[23] Mosayebi A., Abedini R., The Effect of Nanoclay on The Viscosity of Crude Oil, *Adv. Sustain. Petrol. Eng. Sci.*, **3**:147-153 (2011).

[24] Yang E.H., Noh Y.S., Hong G.H., Moon D.J., Combined Steam and CO_2 Reforming of Methane Over $La_{1-x}Sr_xNiO_3$ Perovskite Oxides, *Catal. Today.*, **299**: 242-250 (2018).

[25] Mosayebi A., Kinetic Modeling and Experimental Investigations of Dry Reforming of Methanol over a Cr-Mo-Mn/SiO_2 Catalyst, *Res. Chem. Intermed.*, **47**: 2951-2972 (2021).

[26] Batebi D., Abedini R., Mosayebi A., Combined Steam and CO_2 Reforming of Methane (CSCRM) over Ni–Pd/Al_2O_3 Catalyst for Syngas Formation, *Int. J. Hydrogen. Energy.*, **45**:14293-14310 (2020).

[27] Batebi D., Abedini R., Mosayebi A., Kinetic Modeling of Combined Steam and CO_2 Reforming of Methane over Ni-Pd/Al_2O_3 Catalyst Using Langmuir-Hinshelwood and Langmuir–Freundlich Isotherms, *Ind. Eng. Chem. Res.*, **60**: 851-863 (2021).

[28] Mosayebi A., Abedini R., Bakhshi H., Ni@Pd Nanoparticle with Core-Shell Structure Supported over γ-Al2O3 for Partial Oxidation Process of Butane to Syngas, *Int. J. Hydrogen Energy.*, **42**: 18941-18950 (2017).

[29] Lee S.M., Hwang I.H., Kim S.S., Enhancement of Catalytic Performance of Porous Membrane Reactor with Ni Catalyst for Combined Steam and Carbon Dioxide Reforming of Methane Reaction, *Fuel. Process. Technol.*, **188**:197–202 (2019).

[30] Yu S., Hu Y., Cui H., Cheng Z., Zhou Z., Ni-Based Catalysts Supported on $MgAl_2O_4$ with Different Properties for Combined Steam and CO_2 Reforming of Methane, *Chem. Eng. Sci*., **232**:116379 (2021).

[31] Dan M., Mihet M., Borodi G., Lazar MD., Combined Steam and Dry Reforming of Methane for Syngas Production From Biogas Using Bimodal Pore Catalysts, *Catal. Today*., **366**: 87-96 (2021).

[32] Özkara-Aydinoğ lu S., Thermodynamic Equilibrium Analysis of Combined Carbon Dioxide Reforming with Steam Reforming of Methane to Synthesis Gas, *Int. J. Hydrogen. Energy.*, **35**: 12821–12828 (2010).

[33] Nakhaei Pour A., Mousavi M., Combined Reforming of Methane by Carbon Dioxide and Water: Particle Size Effect of Ni–Mg Nanoparticles, *Int. J. Hydrogen. Energy*, **40**:12985–12992 (2015).

[34] Zhao K., Wang W., Li Z., Highly Efficient Ni/ZrO_2 Catalysts Prepared via Combustion Method for CO_2 Methanation, *J. CO_2. Utili.*, **16**: 236–244 (2016).

[35] Ruckenstein E., Wang H.Y., Carbon Deposition and Catalytic Deactivation During CO_2 Reforming of CH_4 over Co/Al_2O_3 Catalysts, *J. Catal.*, **205**: 289-293 (2002).

[36] Ding C., Ai G., Zhang K., Yuan Q, Han Y, Ma X., Wang J., Liu S., Coking Resistant $Ni/ZrO_2@SiO_2$ Catalyst for the Partial Oxidation of Methane to Synthesis Gas, *Int. J. Hydrogen Energy*, **40**: 6835-6843 (2015).